Milk derived colloid as a novel drug delivery carrier for breast cancer

Masamichi Hayashi[1], Nissim Silanikove[2,3], Xiaofei Chang[1], Rajani Ravi[1], Vui Pham[1], Gilson Baia[4], Keren Paz[4], Mariana Brait[1], *David Sidransky[1]

[1]Department of Otolaryngology-Head and Neck Surgery, Johns Hopkins School of Medicine, Baltimore, MD, USA [2]Department of Molecular & Cellular Physiology, University of Cincinnati, College of Medicine, [3]Biology of Lactation Laboratory, Institute of Animal Science, the Volcani Center, Bet Dagan, Israel. [4]Personalized Oncology, Champions Oncology, Baltimore, MD, USA

***Corresponding author**: David Sidransky, MD

Department of Otolaryngology and Head & Neck Surgery

The Johns Hopkins University School of Medicine

1550 Orleans Street, 5N03, CRB II, Baltimore, MD, 21231, USA

Phone: 410-502-5153, FAX: 410-614-1411, E-mail: dsidrans@jhmi.edu

There is no financial or other interest with regard to the submitted manuscript that might be construed as a conflict of interest.

Abstract

Triple negative breast cancer has an extremely poor prognosis when chemotherapy is no longer effective. To overcome drug resistance, novel drug delivery systems based on nanoparticles have had remarkable success. We produced a novel nanoparticle component 'MDC' from milk-derived colloid. In order to evaluate the anti-cancer effect of MDC, we conducted *in vitro* and *in vivo* experiments on cancer cell lines and a primary tumor derived breast xenograft. Doxorubicin (Dox) conjugated to MDC (MDC-Dox) showed higher cancer cell growth inhibition than MDC alone especially in cell lines with high EGFR expression. In a mouse melanoma model, MDC-Dox significantly suppressed tumor growth when compared with free Dox. Moreover, in a primary tumor derived breast xenograft, one of the mice treated with MDC-Dox showed partial regression, while mice treated with free Dox failed to show any suppression of tumor growth. We have shown that a novel nanoparticle compound made of simple milk-derived colloid has the capability for drug conjugation, and serves as a tumor-specific carrier of anti-cancer drugs. Further research on its safety and ability to carry various anti-cancer drugs into multiple drug-resistant primary breast models is warranted.

Running Title: Milk derived colloid as a nanoparticle

Key Words: milk, nanoparticle, breast cancer, Doxorubicin, Doxil, xenograft

1. Introduction

Breast cancer leads in estimated new cancer cases (29%), and is the second cause of estimated

cancer deaths (15%) in US women [1]. Many novel chemotherapeutic drugs and combinations have been tested in breast cancer. However, survival of advanced aggressive cases is still poor, especially in triple-negative breast cancers (TNBCs) (10-20% of all breast cancers [2, 3]). These types of breast cancer do not express important potential therapeutic targets including receptors for estrogen, progesterone and HER2, resulting in poor overall survival and distant recurrence-free survival. Almost 70% of deaths in TNBCs occurred in the first 5 years following diagnosis compared with only 44% of deaths in other types of breast cancers [3].

One of the strategies to overcome drug resistance is to use an intracellular drug delivery system. Nanoparticles provide a multifunctional delivery platform of chemotherapeutic agents to a variety of cancer cell types. Liposomal carriers below 100 nm in diameter have been widely reported to improve the distribution and tumor accumulation of cancer drugs. Gold nano-particle based drug delivery systems have been extensively studied [4]. The vascular pore cut-off size of human and murine tumors grown in mice was examined by Hobbs et al [5]. The majority of tumors had vascular pores of 380-780 nm in diameter when grown subcutaneously, while no extravasation of any circulating particle between 100-580 nm in diameter was detected in normal tissues model [5]. This means that 100 nm particles, which are too big to extravasate from healthy blood vessel walls, can still easily escape from the leaky and hastily built vessels that feed tumors. Nano-sized micelles are enough large and could be selectively delivered to the neoplasm with reduced extravasation in the normal tissues[6]. Cabral et al also demonstrated the distribution of fluorescence-labelled micelles below 100 nm at 1 hour after intra-venous injection into tumor-bearing mice.

One well-known example of a nano-sized drug in the clinic is Doxil® (Doxil) [7]. Doxil is a drug of

doxorubicin (Dox) confined in liposomes that is sterically stabilized by grafting polyethylene glycol onto the surface [pegylated liposomal doxorubicine (PLD)]. PLD has a circulation half-life of 73.9 hours, whereas Dox has a short half-life of less than 10 min. This prolonged circulation facilitates 10-fold higher intracellular drug concentrations in metastatic sites of breast cancer compared with adjacent normal tissue [8]. Moreover, in a phase III trial of metastatic breast cancer in 2004, PLD reduced the myocardial damage to one-third of the free Dox due to its tumor-selective delivery. However, no survival benefit was obtained when compared with free Dox in the trial [9]. These results indicated that nanoparticles as a drug carrier had the potential for tumor selectivity, but not for intra-nuclear transition of Dox and increased therapeutic effect.

The use of milk proteins as drug delivery vehicles represents a new trend. Two milk proteins that have been already investigated for drug delivery applications are β-lactoglobulin and casein [10]. For instance, Bolisetty et al. generated amyloid fibrils from β-lactoglobulin, and found that their conjugation to metal nanoparticles enhanced cell permeability and toxicity [11]. Haratifar et al. used tea catechin-casein complex to significantly decrease cancer cell proliferation [12]. However, these approaches were not subjected to *in vivo* experiments. We have developed an original nano-sized drug delivery system from milk derived colloid, which is called MDC. In this study, we evaluated its potential anti-cancer effects both *in vitro* and *in vivo* using a primary triple negative tumor derived xenograft.

2. Results

2.1 Characteristics of MDC

The parent molecule of MDC is a component of milk and the micelle size was 60-70nm in diameter (**Figure 1a**). To elucidate how MDC changed its structure after penetrating into the cells and being taken into lysosomes, MDC micelles (**Figure 1b, A**) were exposed to low pH and oxidative environment for 20 hours. As a result, an obvious change to the amyloidal structure (**Figure 1b, B**) was observed. In the next step, MDC marked with Fluorescein isothiocyanate (FITC) was locally injected into a single gland of the mammary glands of lactating mice. Twelve hours later, the animals were sacrificed and biopsies were taken for histological examination. A control microscopic image of the gland treated with PBS demonstrates a section of mammary gland with many intact alveoli that contain milk (**Figure 1c)**. In the contralateral gland treated with MDC, some of the alveoli were lumped or perforated (**Figure 1d, A**). Their lumens were empty of milk and contained many shaded epithelial cells. A massive destruction of the secretory system was also found as a result of complete collapse of alveoli (**Figure 1d, B**) and was associated with intensive penetration of MDC into the cells of the alveolar wall (**Figure 1d, C**). Equivalent level of destruction of the mice mammary gland was typically seen 3 to 7 days after the induction of post-lactational involution [13]. MDC uptake into cell culture was also examined using the HC11 mouse mammary epithelial cell line incubated with MDC marked with FITC. A confocal microscopic picture shows significant intracellular MDC visualized even after 30 minutes of incubation (**Figure 1e, A**). Magnified images taken after 12 hours of incubation clearly demonstrated that the penetration of MDC into the cell was associated with distortion of its normal shape and formation of pseudo-tail (**Figure 1e, B-D**). The penetration of MDC was not limited to a specific region of the cell. Thus, the results suggest that MDC conversion in the lysosome into a toxic substance may lead to

lysosome perforation and release of enzymes into the cell cytoplasm, which is followed by cells death due to autolysis.

2.2 Anti-cancer effect of MDC for breast normal epithelium and cancer cell lines

In order to confirm the anti-cancer effect of MDC against breast cancer cell lines, we used an MTT assay in 2 breast epithelial cell lines (MCF-10A and MCF-12A) and 2 breast cancer cell lines (MDA-MB-231 and MDA-MB-468) using a variety of MDC concentrations (**Figure 2a**). Treatments effects were most obvious at 72 hours post-treatment where cell proliferation rates of MDA-MB-468 was clearly decreased to approximately 40% compared with those of normal epithelial cell lines. However, other cell lines showed no clear inhibition effect. In the next step, we used MDC-Dox (Dox:100 uM) in these cell lines (**Figure 2b**). The cell growth suppression was much greater than MDC alone and was almost completely inhibited at 72 hours in MDA-MB-468. As we confirmed that there was no free Dox in the MDC-Dox, the additional effect of this treatment on suppression of cell growth might be due to the increase of cell toxicity by the Dox conjugation to MDC, or in other words, MDC served as a carrier that introduced Dox into the cell interior. However, the effect of MDC-Dox was also seen in normal cell lines. Also, inhibition rate was widely different between the two cancer cell lines: which indicated that membrane permeability was different. Although both cell lines are triple-negative breast cancers, the expression of epidermal growth factor receptor (EGFR) in MDA-MB-231 is (1+) and that of MDA-MB-468 is (3+) according to a previous paper [14]. In order to further explore the association between MDC effect and EGFR expression, we tested the effect of MDC on another two cell lines,

MCF-7 and BT-474, which have both low EGFR level expressions (1+). MTT results are shown in **Supplementary Figure S1**. Cell toxicity of MDC or MDC-Dox was less clearly seen in these cell lines than in normal epithelial cell lines (MCF-10A and MCF-12A, **Figure 2**) which have moderate EGFR expressions (2+). Thus, our results suggest that MDC contains cluster motifs on its surface that can bind to EGFR, or to molecules closely associated to EGFR, and the anti-cell proliferation ability of MDC seems to be more pronounced in higher EGFR-bearing cells.

2.3 Comparison of Dox conjugated MDC with free Dox in vitro setting

MDC-Dox was also compared with free Dox in *in vitro* experiments. Based on EGFR expression, we used the MDA-MB-453 breast cancer cell line (EGFR zero) [14], MDA-MB-468 breast cancer cell line (EGFR 3+) and A-431 epidermoid carcinoma cell line (EGFR strongly positive) [15] for the MTT assay (**Supplementary Figure S2**). Consistent with the above-described experiments, MDC-Dox effects on cell proliferation were more pronounced in higher EGFR-expressing cell lines (**Supplementary Figure S2 b**). However, MDC-Dox effects and Dox effects on cell proliferation were almost similar, suggesting that Dox can easily penetrate into cells by its hydrophobic nature when Dox directly contacts cells. The equal effects of MDC-Dox and Dox are consistent with the iso-concentration of Dox in the two preparations, and suggest that the phagocytic uptake of MDC-Dox into cells is not inferior to penetration into cells by diffusion of Dox.

2.4 Optimal Dox concentration for the conjugation to MDC

We tried to increase the concentration of Dox (100 uM, 300 uM, 350 uM and 900 uM) conjugated to a constant amount of MDC. The inhibition rates of cell proliferations in MDC-Dox were always superior to MDC alone in various Dox concentrations except for 900 uM (data not shown). However, 900uM of Dox conjugation to MDC failed neither to overcome MDC alone nor to show any tumor growth inhibition. These observations suggest that too much Dox conjugation modified the three-dimensional structure of MDC and prevented it from binding it's ligand to the cell membrane while it still held most of the Dox tightly and thus prevented the toxic effect of free Dox.

2.5 In vivo experiments using a mice melanoma xenograft model

In order to examine whether MDC-Dox has advantage superior anti-cancer effect over free Dox under *in vivo* conditions, we conducted mice experiments. Initially, we applied our drug to B16-F0-luc mice melanoma model on C57BL/6NCR black mice because of the convenience of the homologous tumor. Also, the B16 cell line has good EGFR expression (**Supplementary Figure S3**) [16] and showed favorable sensitivity to MDC-Dox *in vitro* experiment (data not shown). Average tumor volume change of each group (control: PBS, free Dox and MDC-Dox, n=10 respectively) is shown in **Figure 3a**. The dosage of Dox in free Dox and MDC-Dox was 2.5 mg/kg/week, which was just the half of maximal dose for mice. The mice treated with MDC-Dox clearly showed significant tumor growth suppression when compared with free Dox, after day 17. Moreover, tumors in the free Dox group displayed continued growth and larger volumes than control at the end of the experiment. Less tumor growth in the MDC-Dox group was clearly seen in the IVIS images taken

on day 21 (**Figure 3b**) and tumor images taken on day23 (**Figure 3c**). Mice body weight in the MDC-Dox group was significantly lower than Dox alone at the beginning of the experiment; however, no difference in body weight was found later. At the end, Dox alone group showed increased body weight due to larger tumor volume (**Figure 3d**). As a result, mice in the MDC-Dox group had relatively better overall survival than control (P=0.105, log-rank test) and free Dox (P=0.095, log-rank test) (**Figure 3e**). All of mice died of cancer and many of them were euthanized because of oversized tumors. No visible distant metastasis was found at autopsy.

FITC labeled MDC-Dox was injected intravenously into another mouse and euthanized 24 hours later. Tumor tissues and several organs were collected from the mice and observed by fluorescence microscope. As we expected, fluorescence signals were detected in the tumor (**Figure 4a**), but not in the heart tissue (**Figure 4b**) and in the liver tissue (**Figure 4c**). In addition, necrotic cells were abundant around the fluorescence detected area in the tumor (**Figure 4a**). These pictures clearly demonstrate that MDC-Dox was selectively delivered to the tumor.

Lymphocyte phenotyping analysis was performed using locoregional lymph nodes and a spleen of each control (PBS), free Dox and MDC-Dox group after 3 times treatment. One of the main findings of MDC-Dox was the ratio of MDSC (CD11b/GR1/IL4Ra) in lymph nodes. Although MDSC cells usually increase after recurrent Dox injections (70.05), mice in the MDC-Dox conjugate group maintained a low level of MDSC (39.62), which implies that MDC-Dox conjugate had lower influence on drug-induced immune suppression than free Dox (**Supplementary Table S1**). Also, antigen specific T cell activations occurred in

tumor lysate of MDC-Dox group (7.15) just like in that of Dox group (8.47) (**Supplementary Table S2**).

2.6 In vivo experiment using immunodeficient mice with a primary human breast cancer tumorgraft

As the advantage and tumor selectivity of MDC-Dox was demonstrated in the mice melanoma model, we proceeded to apply this reagent to a primary tumor derived human breast cancer model. We selected CTG-0012 (Champions Oncology) with high EGFR expression (**Supplementary Figure S3**) among many breast cancer tumor grafts in the Champions oncology bank. It also demonstrated drug sensitivity to Doxil (TGI: 84%). We thus used Doxil (n=5) as a positive control and compared MDC-Dox (n=4), free Dox (n=5) and free MDC (n=4) treatment in the model. All mice survived at the end of the experiment and were euthanized. Although Dox dosage was only half (2.5mg/kg) of the maximal dose per mouse per week, the Doxil group showed a very favorable tumor suppressive effect (**Figure 5 a,b,c**). On the contrary, tumor sizes increased in the Dox treated mice, suggesting that Doxil liposomes were selectively delivered into the tumors and resulting in tumor growth inhibition. The MDC group (n=4) showed little or no superior tumor growth inhibition when compared with the free Dox group. The MDC-Dox group (n=4) also failed to demonstrate better tumor inhibition than free Dox on average. However, one of the mice in the MDC-Dox group showed a nice partial response (black dot circle in **b**). This partial inhibition is quite synonymous with a partial remission in the clinic. Tumor and organs were excised from the mouse, and Hematoxylin-Eosin staining was performed (**Supplementary Figure S4**). The majority part of tumor was necrotic, and no major organ damage was found. The average body weight (**Figure 5d**) and peripheral blood cell counts (**Supplementary Table S3**)

did not differ between the treatments.

3. Discussion

The recent success of nanoparticles as drug carriers has changed the practice of oncology for some tumor types. One advantage of these drugs may come from their ability to bypass multi-drug resistance (MDR). One of the main mechanisms for drug resistance is activation of efflux pumps that eliminate the drugs from the cells and indeed, P-glycoprotein (Pgp) is known as a major cause of chemotherapy failure. Over expression of Pgp on the cell membrane can actively efflux various anticancer drugs from the cell, and reduce the intracellular drug dose [17]. Since the efflux channel of Pgp is limited to small substrates (300-2000Da) [18], nanoparticles (over 10000Da) can avoid efflux and stay inside the cell thus overcoming MDR at least in theory.

Other mechanisms of resistance to chemotherapy include amplification of genes that help cancer cells to cope with drugs [19] or increase in DNA repair after damage from chemotherapeutic agents [20]. In our case, drug is delivered to the lysosomes by MDC where it induces lysosomal-mediated cell death due to release of enzymes stored in the lysosome. Thus, this type of cell death should also be effective in drug resistant cancer cells with genomic alterations, as the released enzymes will destroy the whole cell interior. Interestingly, lysosomal-mediated cell death is considered as the main mechanism of the massive cells loss that associate with mammary gland involution [21]. Thus, MDC might have a natural role in inducing involution of mammary glands.

The size of the nanoparticle determines its efficiency as a drug carrier. In previous studies, it was found that particles in the range of 60-400nm extravasate and accumulate in tumors via a passive mechanism, called 'enhanced permeability and retention (EPR)' effect [22]. Accordingly, the size of MDC (60-70 nm) or Doxil (80-90 nm [7]) are in the suitable range for inducing the EPR effect. However, only particles in the range of 30 nm in diameter could penetrate into poorly permeable pancreatic tumors [23]. Also, only small molecules (9-40 nm in diameter) can pass through the nuclear envelop if they are to function inside the nucleus envelop [24, 25].

One of the critical characteristics of nanoparticles as a drug delivery system is the ability to lower dose administration and thus toxcicity. This notion is supported by data showing a long resident time in the blood and high tumor-specific delivery for some nanaoparticles. Lu et al examined the pharmacodynamics of pegylated lipopsomal doxorubicine (PL-Dox) and free Dox. The half-life of injected 5mg/kg Dox in mice was twice longer in PL-Dox than free Dox. Moreover, the Dox concentration in stomach, small intestine and heart tissues were significantly reduced. Moreover, the difference in tumor growth inhibition was larger during the administration of a low drug concentration than that of a high concentration [26]. Thus, PL-Dox 50 mg/m^2 every 4 weeks was not inferior to Dox 60 mg/m^2 every 3 weeks in terms of progression free survival for metastatic breast cancer in a phase III clinical trial [9]. Also, low dose administration can be a great advantage for maintaining the same chemotherapy effect while lessening adverse events. PL-Dox 50 mg/m^2 every 4weeks was associated with a significantly lower risk of left ventricular ejection fraction-defined cardiotoxicity than Dox 60 mg/m^2 every 3 weeks [27]. Similarly, in the melanoma model in this study, although just half (2.5mg/kg)

of the maximal Dox dosage (5mg/kg) was administrated to mice, the MDC-Dox conjugated group still showed significant tumor growth inhibition when compared with the free Dox group. Furthermore, the lack of evidence of penetration of MDC-Dox into heart and liver indicates that anti-tumor effects were induced with likely minimal side effects to essential organs.

Another advantage of nanoparticles may be their vessel protection effect in the circulating blood. Dox, like other chemotherapeutic reagent, is potentially harmful to vascular endothelial cells. Bar-Joseph et al. demonstrated that Dox injection in the tail vein of mice decreased ovarian, testicular and femoral blood volume and flow [28]. They also found that vessel walls became irregular and small vessels were gradually diminished implying that general vascular damage could occur anywhere in the body. Theoretically, Dox contained in MDC-Dox is surrounded by colloids derived from milk. Thus, the vascular damage of MDC-Dox is expected to be much lower than free Dox.

In the primary breast tumor graft experiment, the Doxil group showed a distinct anticancer effect when compared with free Dox as expected since Doxil is a proven and marketed drug. This result confirms that nano-sized liposomal molecules can overcome drug resistance. However in the MDC-Dox group, the treatment failed to inhibit tumor growth in 3 out of 4 mice perhaps related to the inability of the conjugates to penetrate the vascularity of the tumor. On the other hand, one mouse in the MDC-Dox group showed significant tumor inhibition which often correlates with a true partial response in the clinic. This result could also be due to the toxicity of the MDC colloid itself when it penetrates tumor cells and thus more tumor models with various sensitivities to Dox have to be tested. In the future, improving the quality of MDC by

reducing its size to the range of 30 nm without losing other qualities may prove an effective way to treat resistant tumors, alone or conjugated to chemotherapeutic drugs.

Our experiments only demonstrated part of the potential broad spectrum applications of MDC. As almost all anti-cancer drugs are highly hydrophobic, MDC can theoretically bind to any existing drug effectively. Actually, we have already verified the capacity of MDC to bind strongly and efficiently to curcumin, daunorubicin and methotrexate. Moreover, as MDC is a protein and capable to undergo ionic covalent interactions, it will be quite easy to develop MDC as a carrier of micro RNA, shRNA and ligands or antibodies of plasma membrane receptors. Thus, MDC might be applied as a universal tumor-specific drug carrier.

In conclusion, we demonstrated that a novel nanoparticle made of milk-derived colloid has an anti-cancer effect and tumor-specific accumulation. The tumor-specific accumulation property of MDC is associated with its particle size and tendency to interact with EGFR which is amplified in many cancer cell lines. Once interacting with the cell membrane, MDC is taken into the lysosomes where it causes lysosome perforation. This property of MDC alone is promising in the treatment of drug resistant cancer lines. Moreover, conjugation of the chemotherapy drug, Dox to MDC increased the tumor suppressive effect *in vivo* without any macro or histological adverse effects. Thus, further studies are warranted to test MDC or MDC conjugates in breast cancer and other types of tumors.

4. **Materials and methods**

4.1 Preparation of Dox conjugated MDC micelles

A colloid made of protein was isolated from milk, which we defined here as MDC. As MDC has the propensity to bind strongly hydrophobic substances, Dox can be firmly bound to MDC by hydrophobic interactions. To determine the binding kinetics of Dox from Dox conjugated MDC (MDC-Dox), 0.5 mL of MDC-Dox solution was placed in a dialysis bag (molecular weight cut-off, 10 kDa) which was incubated in 30 mL of phosphate-buffered solution (pH 7.4) containing Tween 80 (0.5% w/w) at 37°C with gentle shaking for 72 h. Although the Dox molecular weight was much lower than the molecular weight cut-off, there was no leak of Dox from the bag.

4.2 Cell culture

HC11 mouse mammary epithelial cells were cultured at 5% CO_2 in DMEM/F12 (Invitrogen, Carlsbad, CA) supplemented with 10% fetal bovine serum, 10 ng/ml of EGF (Invitrogen), 5 μg/ml of insulin (Sigma-Aldrich, St. Louis, MO), and 1 μg/ml hydrocortisone (Sigma-Aldrich). As for human breast cancer cell lines, MCF-10A cells were cultured with MEGM kit with 100ng/ml of cholera toxin (Sigma-Aldrich) and without GA-1000 (gentamycin-amphotericin B mix). MCF-12A was cultured with DMEM/F12 with 20 ng/ml of EGF, 100ng/ml of cholera toxin, 10ug/ml of bovine insulin, 500ng/ml of hydrocortisone and 5% horse serum. MCF-7, MDA-MB-468, MDA-MB-231, and A-431 was cultured in DMEM medium supplemented with 10% fetal bovine serum and 1% penicillin-streptomycin solution. BT-474 cells were cultured in DMEM/F12 medium supplemented with 10% fetal bovine serum and 1% penicillin-streptomycin solution.

MDA-MB-453 cells were cultured in RPMI medium supplemented with 10% fetal bovine serum and 1% penicillin-streptomycin solution. All cell lines described above were purchased from American Type Culture Collection (Manassas, VA). The B16-F0-luc mice melanoma cell line was purchased from JCRB cell bank (Osaka, Japan) and cultured in DMEM medium supplemented with 10% fetal bovine serum and 1% penicillin-streptomycin solution. All of these cell lines were maintained in a humidified chamber at 37°C in an atmosphere containing 5% CO_2.

4.3 Cell proliferation assay (MTT assay)

The sensitivities to MDC of various breast cancer cell lines were compared by a cell proliferation assay. Each cell line was placed on a 96-well plate at a density of 5-10 x 10^3 cells per well and incubated overnight at 37^0C. Twenty four hours later, several dilutions of Dox conjugated MDC were added to the plate. Cellular viability was measured by the 3-(4, 5-dimethyl thiazol-2-yl)-2, 5-diphenyl tetrazolium bromide (MTT) proliferation assay kit (ATCC) after different time points according to the manufacturer's instructions. Briefly, 10 µl of MTT labeling reagent (5 mg/ml MTT) was added to the culture medium, which was then incubated in the dark for a further 4 h at 37°C. This step was followed by cell lysis with the addition of 100 µl of a detergent reagent. The plates were incubated for 2 h at 37°C to dissolve formazan crystals. Spectrophotometric readings (570nm/650nm) were obtained on a Spectra Max 250 96-well plate reader (Molecular Devices). Each assay was performed in triplicate, and each experiment was repeated at least three times.

4.4 In vivo experiment using mice melanoma tumorgraft on C57BL/6NCR black mice

Mice melanoma cancer B16-F0-luc cells (5×10^5 in 0.1 ml PBS) were implanted subcutaneously in each flank of 5–6 week-old 30 female C57BL/6NCR black mice (NCI at Frederick, Frederick, MD). Mice were housed under standard conditions and had access to food and water ad libitum. All animal protocols were approved by Johns Hopkins University Animal Care and Use Committee and animals were treated in accordance with the Policies and Guidelines of the Committie. The tumor size was measured using a caliper, and the tumor volume was calculated as $\text{width}^2 \times \text{length} \times 0.52$. Seven days later (day 7), tumor growth was observed in all 30 mice and they were randomly divided into 3 groups (Dox, MDC-Dox and Control).

Mice were injected intravenously with free Dox, MDC-Dox or PBS (control) via the tail vein. A dose per injection was 2.5mg/kg Dox, 2.5mg/kg MDC-Dox or the same volume of PBS. This Dox dose was just the half of the maximal Dox administration dose to mice (5.0mg/kg). This dose was determined by the limitation of maximal injection volume of MDC-Dox reagent to mice. Injection was repeated by 4 times (day7, 14, 21and 28). During the whole survival period, tumor size and mouse weight was measured twice a week. To record the survival of the tumor-bearing mice, either natural death or a tumor diameter greater than 2 cm leading to death was considered death. Tumor viability was also measured by intra-peritoneal injection of 50ug/g luciferine using an In Vivo Imaging System (IVIS) (PerkinElmer, Waltham, MA).

4.5 Tissue phenotyping

Spleens, lymph nodes and tumors were collected from B16-F0-luc tumor bearing mice from each treatment group. Spleens and lymph nodes were processed by manual disassociation in RPMI (Invitrogen), and tumor by collagenase digestion. Red blood cells from spleen and tumor were lysed using ACK Red Cell Lysis buffer (MA Bioproducts Boston, MA) for 1 minute at room temperature, and neutralized by the lysis buffer with RPMI containing 10% FBS. The cells were washed at 1500rpm for 10 minutes at 4^0 C, the pellets were re-suspended in RPMI, and the total number of cells was counted.

Cells were stained to identify myeloid-derived suppressor cells (MDSC). Cells were stained extracellularly with GR1 FITC, CD11b APC, CD124 PE and their respective isotypes for 15 minutes at 4^0 C, washed and evaluated by FACS Calibur (BD Biosciences, San Diego, CA), then analyzed with CellQuest Software (BD Biosciences).

Tumor-reactive CD8+ T cells were measured by their antigen specific expression of interferon gamma. To evaluate the expression of interferon gamma on CD8+T cells, spleen cells or lymph node cells were cultured in 96 well plate ($2x10^5$ cells/well) with medium alone, or tumor cell lyste for 72 hours, then incubated with GolgiStop for 3-4 hours at 37 C and harvested for interferon gamma expression. Cells were stained extracellularly with anti-CD4PE and anti-CD8FITC and intracellularly with Interferon Gamma (Permeabilization kit and antibodies from BD Biosciences, San Diego, CA) as described above. The stained cells were evaluated on a FACS Calibur and then analyzed with CellQuest.

4.6 Breast cancer tumor grafts model on immunodeficient mice

Experiments *in vivo* of the breast cancer tumor graft were performed at Champions Oncology (Champions Oncology, Hackensack, NJ), which is accredited and regulated by the Institutional Animal Care and Use Committee (IACUC). The primary human breast cancer tumor graft, CTG-0012 (Champions Oncology) was implanted in the flank of immunodeficient mice for the purpose of propagating the tumor to provide sufficient tumor models for testing (n=20, average tumor volume: 54.16mm^3). Mice were housed under standard conditions and had access to food and water ad libitum. At 168.6 mm^3 average tumor volume, mice were randomized in 4 groups (Dox, MDC, MDC-Dox and Doxil). While tumor growth was observed in all mice, 2 mice were censored due to extremely rapid tumor reduction or growth. Mice were injected intravenously once per week via the tail vein. A dose per injection of each group was 2.5mg/kg Dox, MDC without Dox, 2.5mg/kg Dox containing MDC-Dox or 2.5mg/kg Dox containing Doxil. Injection was performed once per week (day 0, 7, 14, 21, 28 and 35). The drug quantity per injection (2.5mg/kg Dox) was determined by maximal injection volume (200µl/20g mice). During the whole survival period, tumor size and mouse weight was measured twice a week. To record the survival of the tumor-bearing mice, either natural death or an euthanization due to over 2cm tumor was considered death. Tumor dimensions were measured twice weekly by digital caliper and mean estimated tumor volumes ± standard error were graphed for each tumorgraft. Tumor volume (TV) was calculated using the formula: TV=width^2 x length x 0.52.

4.7 Statistical analysis

Continuous values were compared by student's t-tests two tailed. Mouse survival in each group was

compared by Kaplan–Meier curves and log-rank test. P value of <0.05 was considered statistically significant.

All statistical analyses were performed using JMP 9 software (SAS institute, Cary, USA).

Acknowledgement

This work was supported by the NIH grant, Spore in Head and Neck Cancer (P50DE019032) (D. Sidransky).

References

1. Siegel R, Ma J, Zou Z, Jemal A. Cancer statistics, 2014. CA: a cancer journal for clinicians 2014; 64:9-29.
2. Yadav S, Sehrawat A, Eroglu Z, Somlo G, Hickey R, Yadav S, et al. Role of SMC1 in overcoming drug resistance in triple negative breast cancer. PLoS One 2013; 8:e64338.
3. Dent R, Trudeau M, Pritchard KI, Hanna WM, Kahn HK, Sawka CA, et al. Triple-negative breast cancer: clinical features and patterns of recurrence. Clin Cancer Res 2007; 13:4429-34.
4. Lee J, Chatterjee DK, Lee MH, Krishnan S. Gold nanoparticles in breast cancer treatment: promise and potential pitfalls. Cancer Lett 2014; 347:46-53.
5. Hobbs SK, Monsky WL, Yuan F, Roberts WG, Griffith L, Torchilin VP, et al. Regulation of transport pathways in tumor vessels: role of tumor type and microenvironment. Proc Natl Acad Sci U S A 1998; 95:4607-12.
6. Rapoport N, Gao Z, Kennedy A. Multifunctional nanoparticles for combining ultrasonic tumor imaging and targeted chemotherapy. J Natl Cancer Inst 2007; 99:1095-106.
7. Soundararajan A, Bao A, Phillips WT, Perez R, 3rd, Goins BA. [(186)Re]Liposomal doxorubicin (Doxil): in vitro stability, pharmacokinetics, imaging and biodistribution in a head and neck squamous cell carcinoma xenograft model. Nuclear medicine and biology 2009; 36:515-24.
8. Symon Z, Peyser A, Tzemach D, Lyass O, Sucher E, Shezen E, et al. Selective delivery of doxorubicin to patients with breast carcinoma metastases by stealth liposomes. Cancer 1999; 86:72-8.
9. O'Brien ME, Wigler N, Inbar M, Rosso R, Grischke E, Santoro A, et al. Reduced cardiotoxicity and comparable efficacy in a phase III trial of pegylated liposomal doxorubicin HCl (CAELYX/Doxil) versus conventional doxorubicin for first-line treatment of metastatic breast cancer. Ann Oncol 2004; 15:440-9.
10. Lohcharoenkal W, Wang L, Chen YC, Rojanasakul Y. Protein nanoparticles as drug delivery carriers for cancer therapy. BioMed research international 2014; 2014:180549.

11. Bolisetty S, Boddupalli CS, Handschin S, Chaitanya K, Adamcik J, Saito Y, et al. Amyloid fibrils enhance transport of metal nanoparticles in living cells and induced cytotoxicity. Biomacromolecules 2014; 15:2793-9.

12. Haratifar S, Meckling KA, Corredig M. Antiproliferative activity of tea catechins associated with casein micelles, using HT29 colon cancer cells. Journal of dairy science 2014; 97:672-8.

13. Lund LR, Romer J, Thomasset N, Solberg H, Pyke C, Bissell MJ, et al. Two distinct phases of apoptosis in mammary gland involution: proteinase-independent and -dependent pathways. Development 1996; 122:181-93.

14. Subik K, Lee JF, Baxter L, Strzepek T, Costello D, Crowley P, et al. The Expression Patterns of ER, PR, HER2, CK5/6, EGFR, Ki-67 and AR by Immunohistochemical Analysis in Breast Cancer Cell Lines. Breast cancer : basic and clinical research 2010; 4:35-41.

15. Tan Y, Chiow KH, Huang D, Wong SH. Andrographolide regulates epidermal growth factor receptor and transferrin receptor trafficking in epidermoid carcinoma (A-431) cells. British journal of pharmacology 2010; 159:1497-510.

16. Xu Q, Zhang X, Yue J, Liu C, Cao C, Zhong H, et al. Human TGFalpha-derived peptide TGFalphaL3 fused with superantigen for immunotherapy of EGFR-expressing tumours. BMC biotechnology 2010; 10:91.

17. Qiu L, Chen T, Ocsoy I, Yasun E, Wu C, Zhu G, et al. A Cell-Targeted, Size-Photocontrollable, Nuclear-Uptake Nanodrug Delivery System for Drug-Resistant Cancer Therapy. Nano letters 2014.

18. Ambudkar SV, Kimchi-Sarfaty C, Sauna ZE, Gottesman MM. P-glycoprotein: from genomics to mechanism. Oncogene 2003; 22:7468-85.

19. Li Y, Zou L, Li Q, Haibe-Kains B, Tian R, Li Y, et al. Amplification of LAPTM4B and YWHAZ contributes to chemotherapy resistance and recurrence of breast cancer. Nature medicine 2010; 16:214-8.

20. Park YY, Jung SY, Jennings NB, Rodriguez-Aguayo C, Peng G, Lee SR, et al. FOXM1 mediates Dox resistance in breast cancer by enhancing DNA repair. Carcinogenesis 2012; 33:1843-53.

21. Kreuzaler PA, Staniszewska AD, Li W, Omidvar N, Kedjouar B, Turkson J, et al. Stat3 controls lysosomal-mediated cell death in vivo. Nature cell biology 2011; 13:303-9.

22. O'Neal DP, Hirsch LR, Halas NJ, Payne JD, West JL. Photo-thermal tumor ablation in mice using near infrared-absorbing nanoparticles. Cancer Lett 2004; 209:171-6.

23. Cabral H, Matsumoto Y, Mizuno K, Chen Q, Murakami M, Kimura M, et al. Accumulation of sub-100 nm polymeric micelles in poorly permeable tumours depends on size. Nature nanotechnology 2011; 6:815-23.

24. Gorlich D, Kutay U. Transport between the cell nucleus and the cytoplasm. Annual review of cell and developmental biology 1999; 15:607-60.

25. Hetzer MW. The nuclear envelope. Cold Spring Harbor perspectives in biology 2010; 2:a000539.

26. Lu WL, Qi XR, Zhang Q, Li RY, Wang GL, Zhang RJ, et al. A pegylated liposomal platform: pharmacokinetics, pharmacodynamics, and toxicity in mice using doxorubicin as a model drug. Journal of pharmacological sciences 2004; 95:381-9.

27. Lyseng-Williamson KA, Duggan ST, Keating GM. Pegylated liposomal doxorubicin: a guide to its use in various malignancies. BioDrugs : clinical immunotherapeutics, biopharmaceuticals and gene therapy 2013; 27:533-40.
28. Bar-Joseph H, Ben-Aharon I, Tzabari M, Tsarfaty G, Stemmer SM, Shalgi R. In vivo bioimaging as a novel strategy to detect doxorubicin-induced damage to gonadal blood vessels. PLoS One 2011; 6:e23492.

Figure legends

Figure 1 a: Electron microscope image of milk-derived colloid (MDC). The image shows that MDC is a colloid-like substance with a diameter in the range of 60-70nm. **b**: MDC is converted from colloidal round shape (**A**) to amyloidal structure (**B**) after the incubation under low pH, or an oxidative environment for 20 hours. This conversion in the lysosome probably induces lysosome perforation. **c:** Image of mammary gland of lactating wild mice is shown at 12 hours after treatment with PBS (control). Many fat droplets (milk) are seen in alveoli. **d**: Images of contralateral mammary gland of the control are shown at 12 hours after treatment with MDC conjugated with Fluorescein isothiocyanate (FITC). Some of the alveoli were lumped or perforated (**Figure 1d, A**). Their lumens were empty of milk and contained abundant shaded epithelial cells. A massive destruction of the secretory system was also found as a result of complete collapse of alveoli (**Figure 1d, B**) and was associated with intensive penetration of MDC into the cells of the alveolar wall (**Figure 1d, C**).**e**: HC11 mice mammary epithelial cells were incubated with MDC conjugated with FITC. Confocal microscopy showed significant intracellular MDC visualized only even after 30 minutes of incubation (**Figure 1e, A**). Magnified images taken after 12 hours of incubation clearly demonstrated that the penetration of MDC into the cell was associated with distortion of its normal shape and formation of a pseudo-tail (**Figure 1e, B-D**).

Figure 2 a: MDC anti-cell proliferation effects on breast epithelial cell lines (MCF-10A and MCF-12A) and cancer cell lines (MDA-MB-231 and MDA-MB-468) were measured by the MTT assay. X-axis shows various MDC dilutions and the y-axis cell proliferation rate (%, average ± standard error), which was calculated by the formula: 100 x (absorbance of tested sample)/(absorbance of control sample of the same time). MDC cell growth inhibition effects were observed in cancer cell lines when compared with those in normal cell lines. **b:** Dox (100uM) conjugated MDC was also tested in the same cell lines by the MTT assay. Although inhibition was clearly apparent in cancer cells, normal cells also showed a significant decrease with Dox conjugated MDC.

Figure 3 *In vivo* effects in a melanoma mouse model a: Average tumor volume and standard error in each group (blue: control (PBS), red: Dox, green: MDC-Dox) are shown. Drug injections were performed on day7, 14, 21, 28. The MDC-Dox group showed significantly slower tumor growth (P value: MDC-Dox versus Dox, student's t-test). **b:** Tumor cells (B16-F0-luc) were labeled with luciferase. After intra-peritoneal injection of luciferin, representative fluorescence images of each group were taken by IVIS on day 21. Relatively small intensities were detected in the MDC-Dox group. **c:** Representative tumor pictures in each group were taken on day 23. Relatively small tumors were visible in the MDC-Dox mice group. **d:** Average body weight of each group is shown. While the MDC-Dox group showed body weight loss at first, no significant difference was found between each group later (P value: MDC-Dox versus Dox, student's t-test). **e:** Kaplan-Meier curves

for overall survival are shown (blue: control (PBS), red: Dox, green: MDC-Dox). The MDC-Dox group had a tendency toward favorable prognosis when compared with the Dox group (P=0.095, log-rank test) and control group (P=0.105, log-rank test).

Figure 4 FITC labeled MDC-Dox was injected into a mouse. Twenty-four hours later, the mouse was euthanized, and images of tumor (**a**), heart (**b**) and liver (**c**) were taken under the fluorescence microscope (x40 and x100, respectively). In the tumor tissue, FITC was clearly detected in the viable cancer cells which were surrounded by a large necrotic area. On the other hand, no fluorescence was detected in the heart and liver.

Figure 5 *In vivo* effects in a primary human breast cancer model. Tumor volumes were plotted on panel **a**, and pictures at day 56 were shown in panel **b**. Although the Dox dosage was only half (2.5mg/kg) of the maximal dose per mouse per week, the Doxil group (n=5) showed a favorable tumor inhibitory effect. On the contrary, the Dox group (n=5) showed an apparent increase in tumor size. The MDC group (n=4) showed little or no superior tumor growth inhibition when compared with the free Dox group. The MDC-Dox group (n=4) also failed to demonstrate better tumor inhibition than free Dox on average (**c**). However, one of the mice in the MDC-Dox group showed a nice partial response (black dot circle in **b**). Average body weights of each group are shown. No significant difference was found in average body weights between groups (**d**).

Figure 1

a. Image of MDC

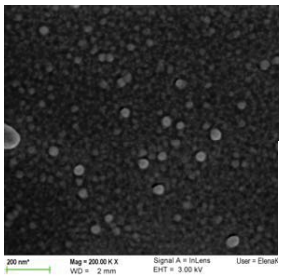

b. Structure change

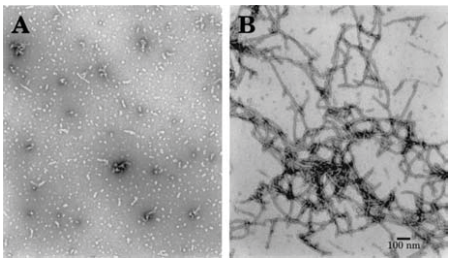

c. Control

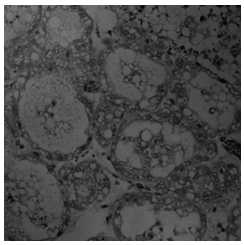

d. MDC injection to mice mammary glands

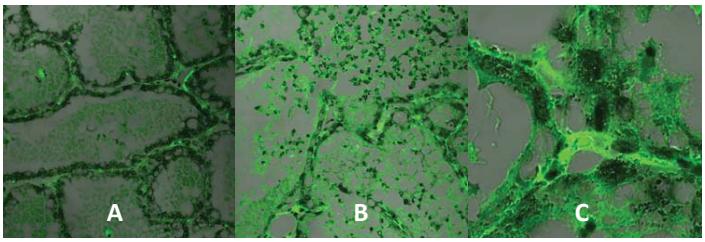

e. HC11 cell line incubation with MDC

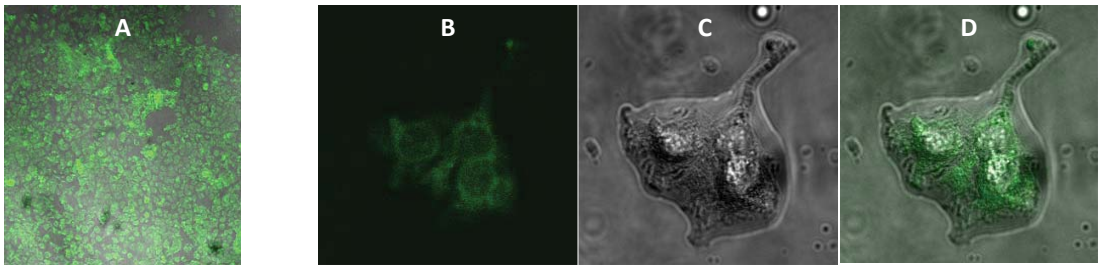

Figure 2

a. MDC effects on breast epithelial and cancer cell lines (MTT assay)

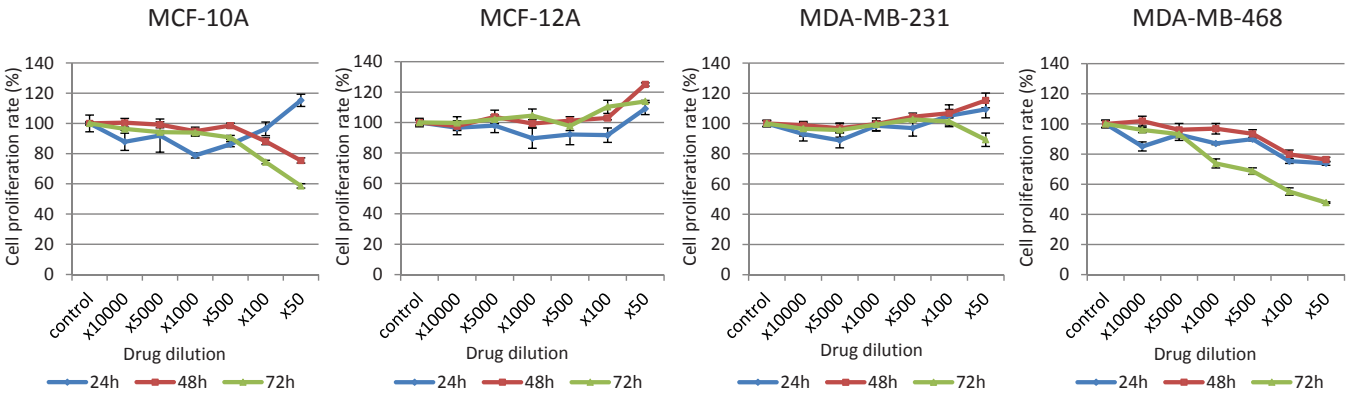

b. MDC-Dox (100uM) effects on breast epithelial and cancer cell lines (MTT assay)

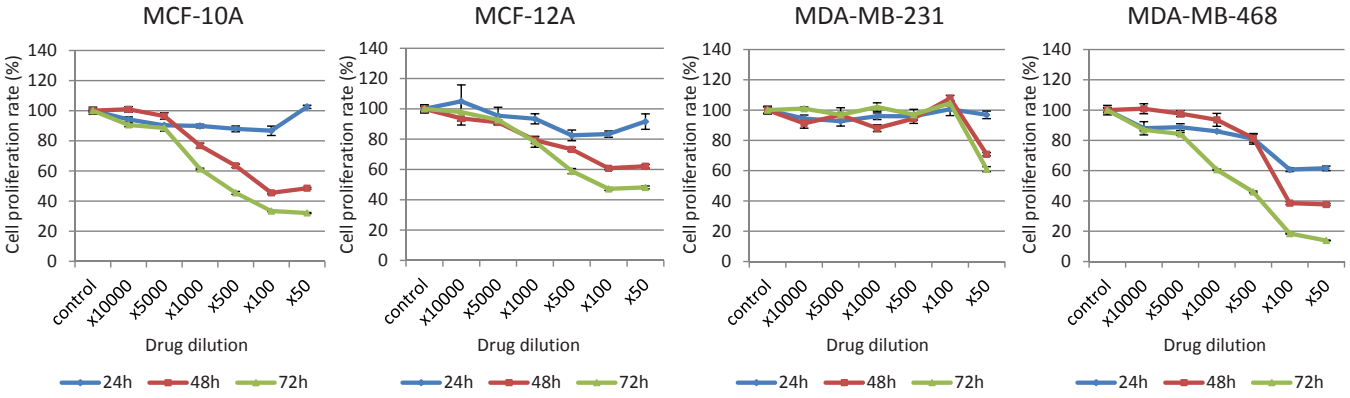

Figure 3

a. Average tumor volume

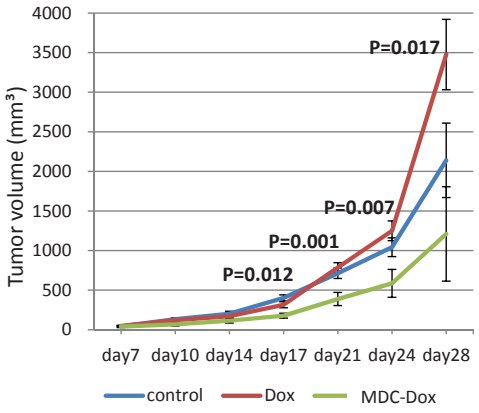

b. Representative tumors (day 21)

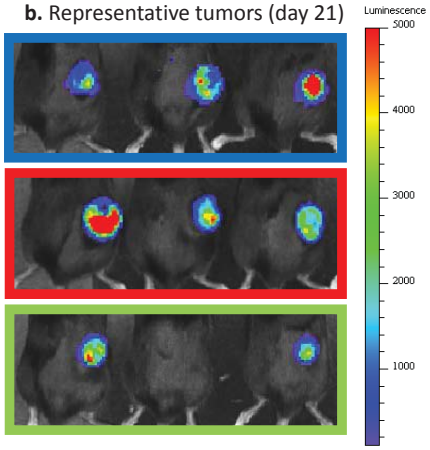

c. Representative tumors (day 23)

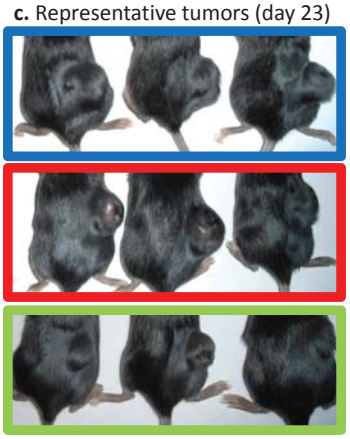

d. Average body weight

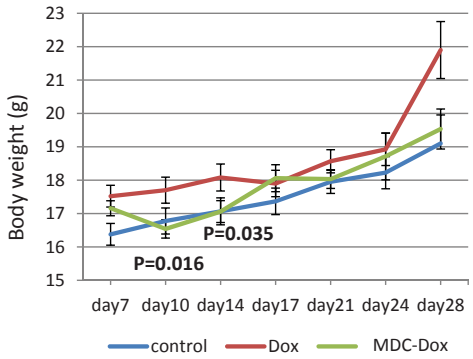

e. Kaplan-Meier curves for overall survival

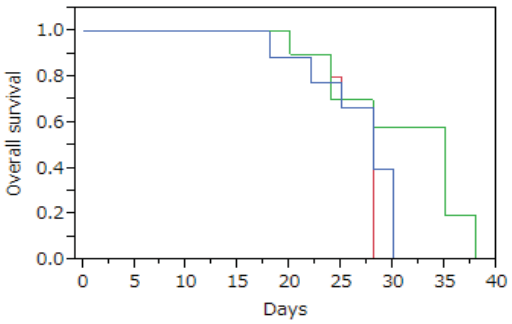

group	P value
Control vs Dox	0.329
Control vs MDC-Dox	0.105
Dox vs MDC-Dox	0.095

Figure 4

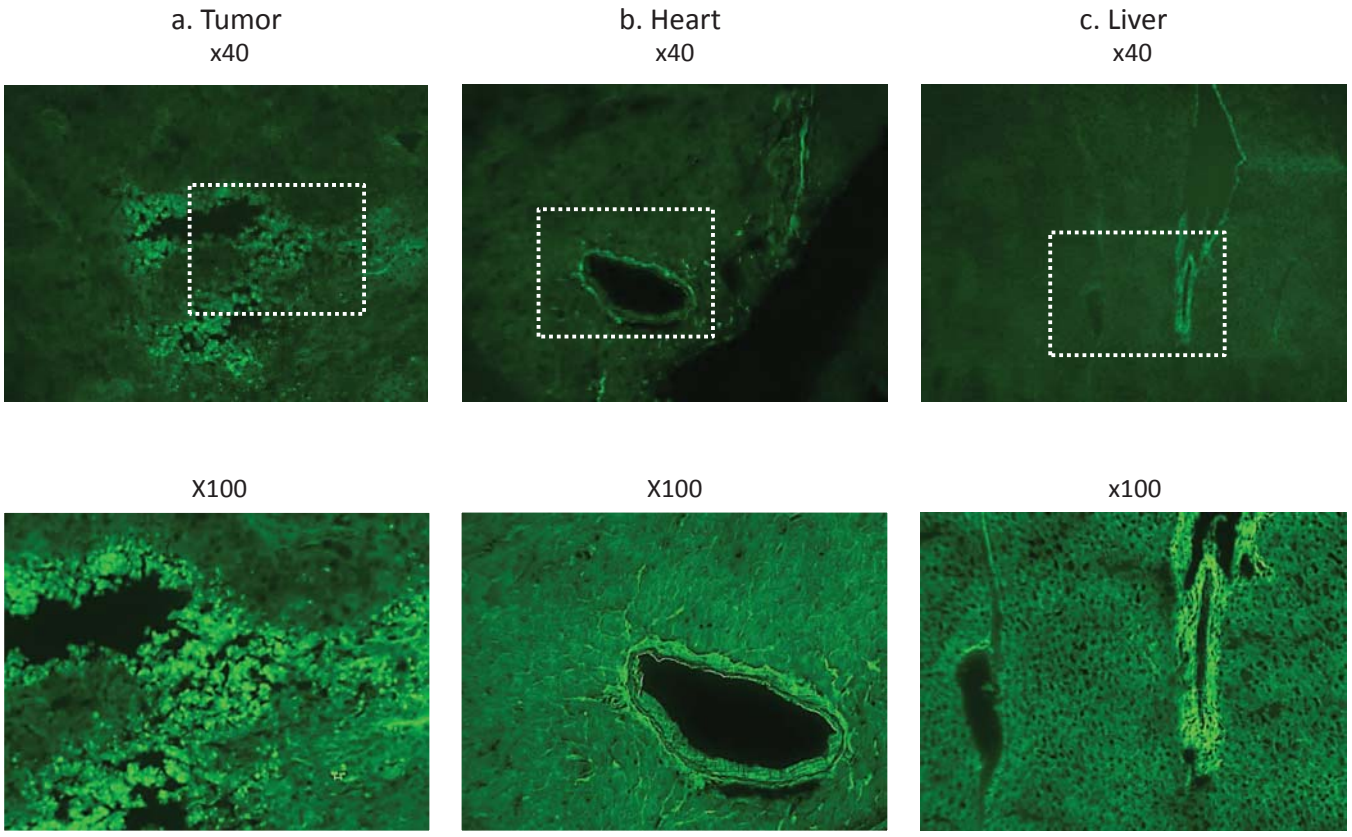

Figure 5

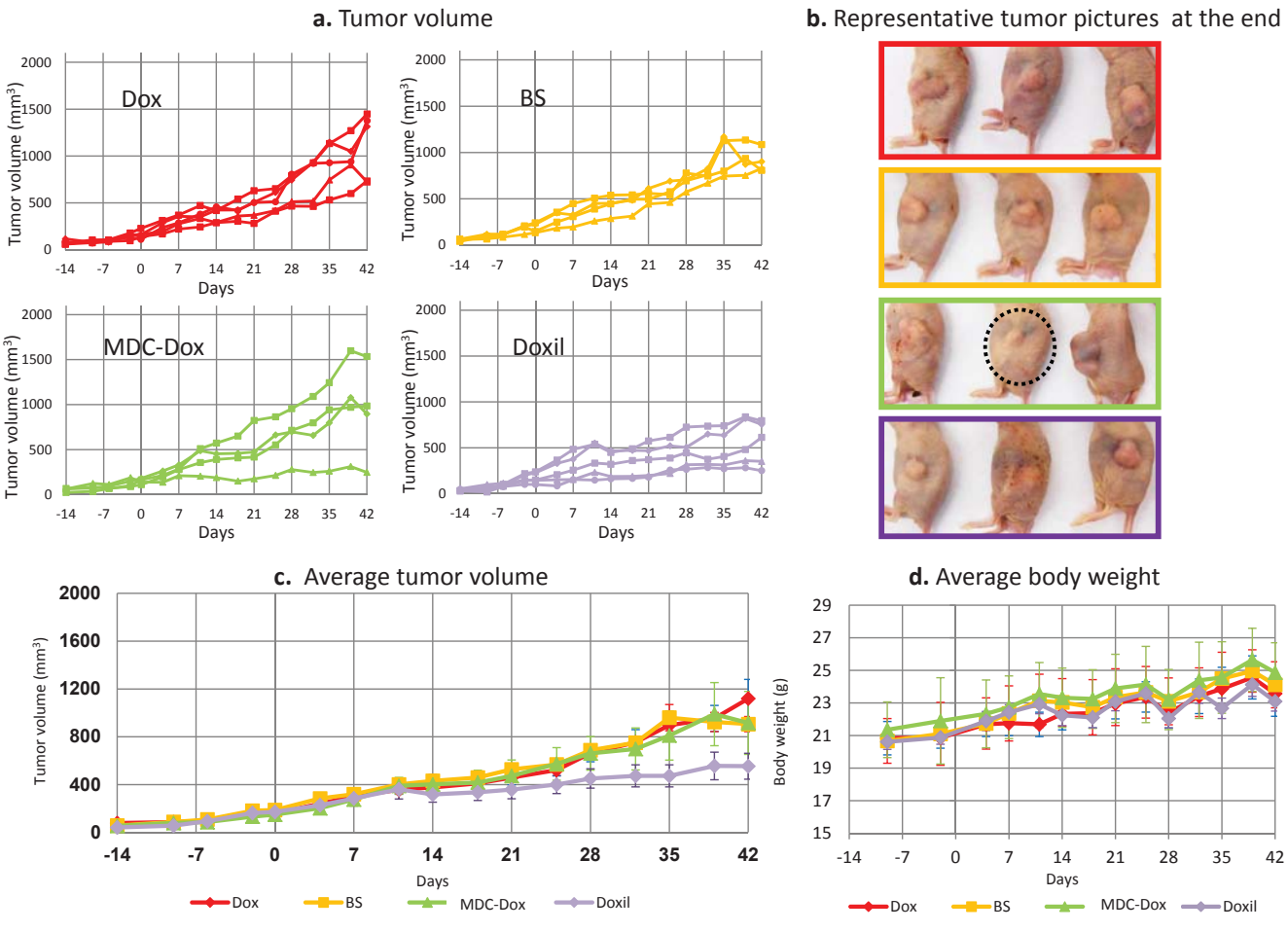
a. Tumor volume
Dox
BS
MDC-Dox
Doxil
Tumor volume (mm³)
Days
b. Representative tumor pictures at the end
c. Average tumor volume
d. Average body weight
Body weight (g)
Dox
BS
MDC-Dox
Doxil

Supplementary Table S1 Lymphocyte phenotyping 1

Lymph node (%)			
	CD4	CD8	CD11b/GR1/IL4Ra+
Control	32.75	31.33	46.5
Dox	24.15	21.82	70.05
MDC-Dox	22.54	17.15	39.62
Spleen (%)			
	CD4	CD8	CD11b/GR1/IL4Ra+
Control	6.34	5.09	52.97
Dox	14.76	9.44	65.59
MDC-Dox	17.93	9.96	74.69

Supplementary Table S2 Lymphocyte phenotyping 2

Medium (%)		
	CD4/IFNg+	CD8/IFNg+
Control	0	0
Dox	0	0
MDC-Dox	0	0
Tumor lysate (%)		
	CD4/IFNg+	CD8/IFNg+
Control	1.11	1.76
Dox	9.07	8.47
MDC-Dox	7.85	7.15

Supplementary Table S3 Average peripheral blood cell counts

		Dox (n=5)	BS (n=5)	MDC-Dox (n=4)	Doxil (n=5)
WBC	K/uL	5.53	4.40	3.97	3.97
NE#	K/uL	2.88	2.69	1.96	2.46
LY#	K/uL	2.47	1.49	1.62	1.39
MO#	K/uL	0.14	0.14	0.16	0.07
EO#	K/uL	0.03	0.07	0.19	0.04
BA#	K/uL	0.01	0.02	0.05	0.01
NE%	%	51.91	58.35	51.62	61.88
LY%	%	44.75	36.88	41.22	35.04
MO%	%	2.57	3.27	3.24	1.83
EO%	%	0.57	1.21	3.11	0.95
BA%	%	0.21	0.29	0.82	0.30
RBC	M/uL	9.73	9.26	9.20	8.24
HB	g/dL	13.42	12.44	12.68	12.48
HCT	%	47.08	43.52	44.98	44.60
MCV	fL	48.40	46.98	48.88	54.12
MCH	Pg	13.80	13.44	13.80	15.14
MCHC	g/dL	28.54	28.60	28.15	27.98
RDW	%	19.22	20.12	19.85	20.40
PLT	K/uL	591.00	535.40	561.50	473.80
MPV	fL	5.56	5.50	4.95	5.30
PDW	%	0.00	0.00	0.00	0.00

Supplementary Figure S1 MDC and MDC-Dox effects on other breast cancer cell lines with low EGFR expression were examined (**a:** MDC, **b:** MDC-Dox). X-axis shows various MDC dilutions and the y-axis cell proliferation rate (%, average ± standard error), which was calculated by the formula: 100 x (absorbance of tested sample)/(absorbance of control sample of the same time). Cell proliferation in both cell lines was not clearly decreased when compared with other cell lines with higher EGFR expression.

Supplementary Figure S2 Dox and MDC-Dox were compared using EGFR positive cell lines (A431 and MDA-MB-468) and an EGFR negative cell line (MDA-MB-453). X-axis shows various MDC dilutions and the y-axis cell proliferation rate (%, average ± standard error), which was calculated by the formula: 100 x (absorbance of tested sample)/(absorbance of control sample of the same time). MDC-Dox showed equal or less cell growth inhibition in all cell lines in this vitro experiment.

Supplementary Figure S3

Western blotting analysis of EGFR protein was performed. Primary and secondary antibodies were purchased from Cell Signaling Technology (Danvers, MA). EGFR expression of breast cancer tumor graft and B16-F0-luc were examined. A453 cell line was used as an EGFR negative control. ACTB was used as a reference (Sigma-Aldrich).

Supplementary Figure S4

Tumor pictures of representative responders in the Doxil group and the MDC-Dox group are shown. **a**:The majority of the tumor area was necrotic. **b**: Representative organs of MDC-Dox group are shown. No visible damage was detected in the liver and lung.

Supplementary Figure S1

a. MDC effects on breast epithelial and cancer cell lines (MTT assay)

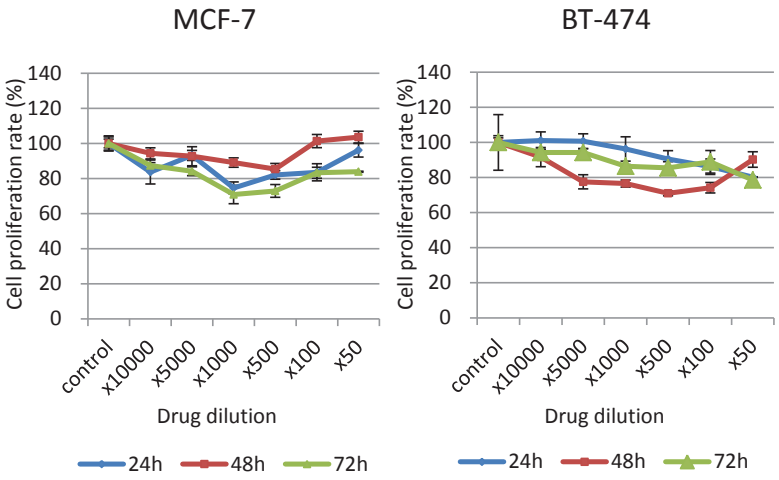

b. MDC-Dox (100uM) effects on breast epithelial and cancer cell lines (MTT assay)

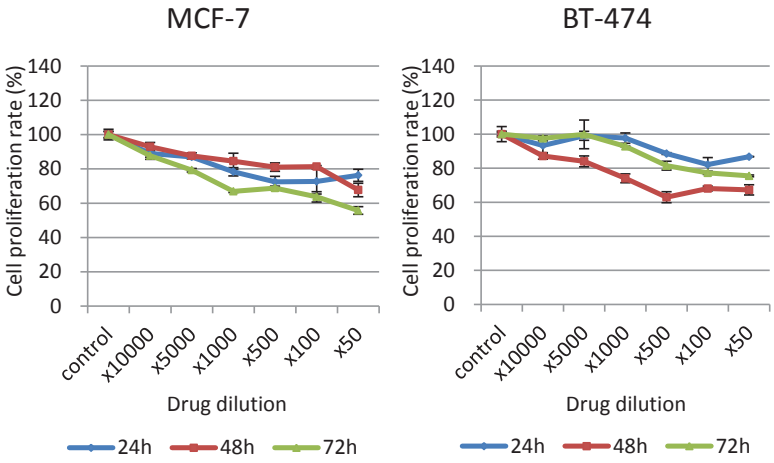

Supplementary Figure S2

a. Dox (100uM) alone effects on cancer cell lines (MTT assay)

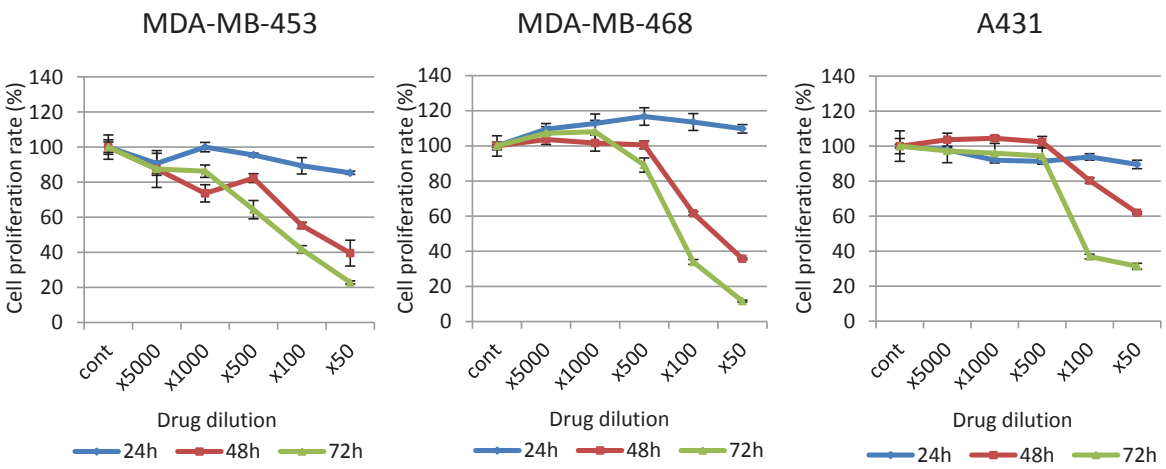

b. MDC-Dox (100uM) effects on breast epithelial and cancer cell lines (MTT assay)

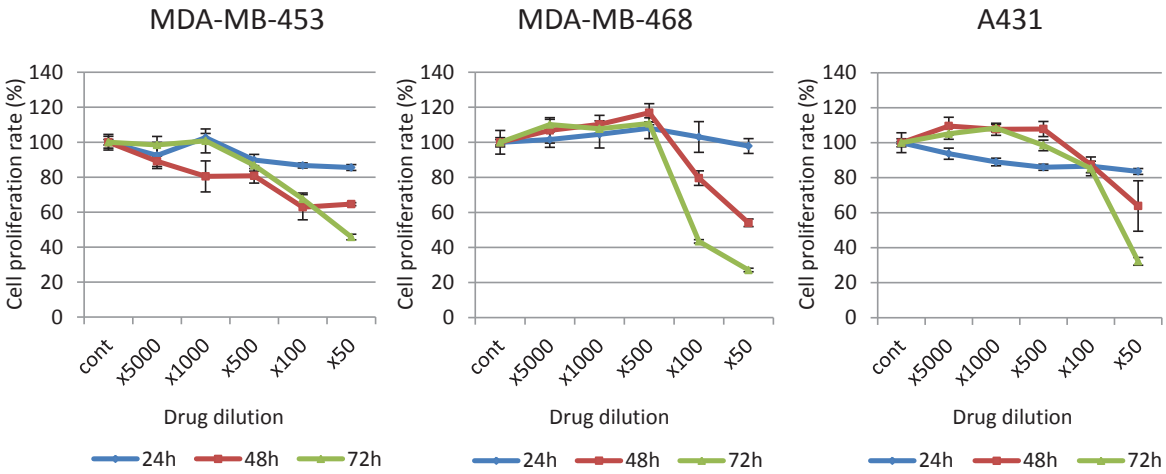

Supplementary Figure S3

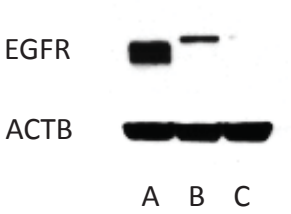

A: Breast cancer tumor graft
B: B16-F0-luc
C: A453

Supplementary Figure S4

a. Tumors (Responder) (H.E. macro, x40)

Doxil

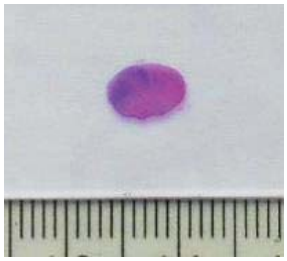

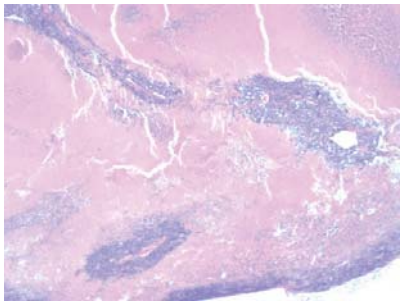

BS-Dox

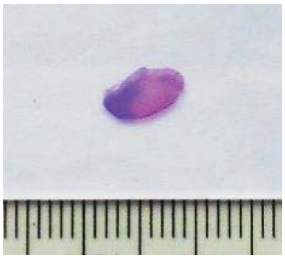

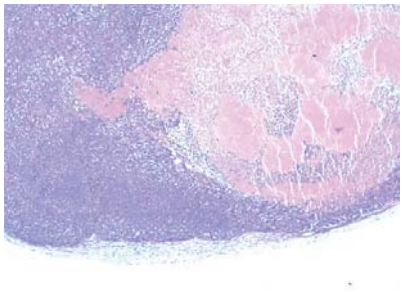

b. Organs in MDC-Dox group (H.E.x40)

Liver

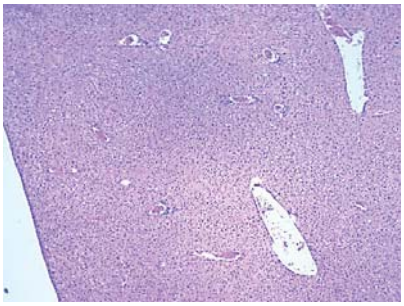

Lung